

## RESEARCH ARTICLE

# Aberrant expression profiles and bioinformatic analysis of CAF-derived exosomal miRNAs from three moderately differentiated supraglottic LSCC patients

Chunping Wu<sup>1</sup> | Mei Wang<sup>2</sup> | Qiang Huang<sup>1</sup> | Yang Guo<sup>1</sup> | Hongli Gong<sup>1</sup> |  
Chunyan Hu<sup>3</sup> | Liang Zhou<sup>1</sup> 

<sup>1</sup>Department of Otorhinolaryngology  
Head and Neck Surgery, Shanghai  
Key Clinical Disciplines of  
Otorhinolaryngology, Eye & ENT Hospital  
of Fudan University, Shanghai, China

<sup>2</sup>Department of Otolaryngology, Shanghai  
Municipal Hospital of Traditional Chinese  
Medicine, Shanghai University of  
Traditional Chinese Medicine, Shanghai,  
China

<sup>3</sup>Department of Pathology, Eye & ENT  
Hospital of Fudan University, Shanghai,  
China

## Correspondence

Liang Zhou, Department of  
Otorhinolaryngology Head and Neck  
Surgery, Eye & ENT Hospital of Fudan  
University, 83 Fenyang Road, Shanghai  
200031, China.  
Email: zhoulent@126.com

## Funding information

National Natural Science Foundations  
of China, Grant/Award Number:  
81972529; Natural Science Foundation  
of Shanghai University of Traditional  
Chinese Medicine, Grant/Award Number:  
2019LK029

## Abstract

**Background:** Aberrant expression of exosomal miRNAs has emerged as a research hotspot. However, no studies have been conducted on the dysregulation of exosomal miRNAs derived from cancer-associated fibroblasts (CAFs) in supraglottic laryngeal squamous cell carcinoma (SLSCC).

**Methods:** Cancer-associated fibroblasts and paired normal fibroblasts (NFs) from SLSCC patients were cultured, and exosomes in the culture supernatants were collected and identified. Exosomal miRNA expression was compared in each pair of CAFs and NFs by next-generation sequencing, and expression of selected exosomal miRNAs was validated by reverse transcription-quantitative PCR. Four online bioinformatic algorithms predicted the potential target genes of aberrantly expressed miRNAs, while gene ontology and Kyoto Encyclopaedia of Genes and Genomes (KEGG) pathway enrichment and network analysis identified downstream target genes and their interactions.

**Results:** Three pairs of CAFs and NFs were successfully cultured and purified. CAF-derived exosomal miRNAs were mostly downregulated and included *miR-656-3p*, *miR-337-5p*, *miR-29a-3p* and *miR-655-3p*; however, some, including *miR-184-3p*, *miR-92a-1-5p*, *miR-212-3p* and *miR-3135b*, were upregulated. Bioinformatics analysis revealed involvement of these miRNAs in biological processes, cellular components and molecular functions. KEGG analysis revealed the top 30 pathways involvement in cancer initiation and progression and in cell cycle regulation. An interaction network showed *miR-16-5p*, *miR-29a-3p*, *miR-34c-5p*, *miR-32-5p* and *miR-490-5p* as the top five miRNAs and *CCND1*, *CDKN1B*, *CDK6*, *PTEN* and *FOS* as the top five target genes.

**Conclusions:** SLSCC patients showed aberrant expression of CAF-derived exosomal miRNAs. The top five miRNAs and their target genes may jointly constitute a carcinogenic tumour microenvironment and act as biomarkers for SLSCC intervention.

Chunping Wu and Mei Wang contributed equally to this work.

This is an open access article under the terms of the Creative Commons Attribution-NonCommercial-NoDerivs License, which permits use and distribution in any medium, provided the original work is properly cited, the use is non-commercial and no modifications or adaptations are made.

© 2021 The Authors. *Journal of Clinical Laboratory Analysis* published by Wiley Periodicals LLC.

**KEYWORDS**

cancer-associated fibroblast, exosome, laryngeal squamous cell carcinoma, miRNAs, supraglottic

## 1 | INTRODUCTION

Supraglottic laryngeal squamous cell carcinoma (SLSCC) is a special type of laryngeal cancer that is prone to lymph node metastasis and post-therapeutic relapse.<sup>1</sup> Tumour relapse is mainly caused by a disordered tumour microenvironment (TME),<sup>2</sup> caused in part by the pro-tumourigenic capacity of cancer-associated fibroblasts (CAFs).<sup>3</sup> CAFs produce extensive exosomes that regulate the TME and direct the growth and progression of cancer cells.<sup>4</sup> Exosomes carry a variety of bioactive molecules, including miRNAs, signal peptides, lipids and DNA.<sup>5</sup> Of these molecules, the exosomal miRNAs play an important role in the modulation of the TME, and the aberrant expression of the exosome-derived miRNAs in CAFs is recognised as important contributors to cancer progression and metastasis.<sup>6</sup>

There is already ample literature on the subject of CAF-derived exosomal miRNAs in many solid tumours,<sup>7,8</sup> and also miRNAs<sup>9,10</sup> and serum exosomal miRNAs<sup>11,12</sup> have been intensively investigated in LSCC. We previously reported that CAFs and conditioned medium (CM) from CAFs derived from LSCC patients could significantly enhance the capacity of proliferation, migration and tumourigenicity of LSCC cells.<sup>13,14</sup> We speculated that CAF-derived exosomal miRNAs may play a key role in this tumour-promoting effect. In addition, we investigated the exosomal miRNAs expression profile derived from LSCC cell line.<sup>15</sup> However, to date, no studies have been conducted to explore the aberrant expression profiles of CAF-derived exosomal miRNAs in patients with LSCC.

In the present study, the aberrant expression profiles of exosomal miRNAs from the three pairs of CAFs and normal fibroblasts (NFs) from different SLSCC patients were identified using next-generation sequencing. Most of the dysregulated exosomal miRNAs were downregulated, including *miR-656-3p*, *miR-337-5p*, *miR-29a-3p*, *miR-655-3p*, *miR-16-5p*, *miR-34c-5p*, *miR-32-5p* and *miR-490-5p*. A few dysregulated exosomal miRNAs were upregulated, including *miR-184-3p*, *miR-92a-1-5p*, *miR-212-3p*, *miR-3135b*, *miR-1306-3p*, *miR-7704* and *miR-1306-3p*. The potential downstream target genes and their interactions with these selected exosomal miRNAs were explored by online bioinformatics analysis. Taken together, our findings indicate that SLSCC patients manifest aberrant expression of CAF-derived exosomal miRNAs. These dysregulated miRNAs and their target genes are mainly related to cell cycle regulation and may play critical roles in SLSCC initiation and progression, providing new insights for the treatment of SLSCC.

## 2 | MATERIALS AND METHODS

### 2.1 | Patient information

Ten tumour specimens from 10 male patients with SLSCC diagnosed by biopsy and pathology were collected immediately after surgical tumour resection. All 10 specimens were classified as moderately differentiated epiglottic LSCC. Paired adjacent normal connective tissues were obtained simultaneously from each patient. Data including laryngoscopic photos, contrast-enhanced computed tomography (CT) scans and pathological photos were also collected.

### 2.2 | Primary culture of tumour specimens and paired adjacent connective tissues

Each SLSCC specimen collected from fresh resected tumours was immersed immediately in cold RPMI 1640 medium (Invitrogen). The specimen was then immersed in povidone-iodine solution (saline-diluted, 1:10, 5 min), followed by gentamycin sulphate solution (saline-diluted, 1:8, 5 min) and finally lincomycin hydrochloride solution (saline-diluted, 1:8, 5 min). The specimen was then washed with phosphate-buffered saline (PBS) and scissored into fragments (1–2 mm<sup>3</sup>). The fragments were trypsinised in RPMI 1640 medium containing type IV collagenase (200 U/ml, Sigma) for 12 h at 37°C. The digested fragments were suspended in bronchial epithelial cell growth medium (BEGM; Catalogue #CC-3170; Lonza) supplemented with 1% penicillin/streptomycin and 10% foetal bovine serum (FBS; Gibco, Life Technologies Corporation). The suspension was plated in 6-cm Petri dishes (Corning Inc.) and incubated for 3–7 days in a humidified incubator in 5% CO<sub>2</sub> at 37°C. The dishes were then examined under a phase-contrast microscope, and any contaminated dishes were discarded. The CAFs that grew successfully without contamination were collected and subcultured.

The paired adjacent connective tissue from the same patient was cultured using this same procedure and served as a control. Primary CAF and NF cultures were successfully generated from tissues from three of the 10 patients.

### 2.3 | Morphological examination and immunocytochemical staining of CAFs and NFs

Cancer-associated fibroblasts and NFs were separated and purified by brief exposure to 0.25% trypsin-EDTA (Invitrogen).

Representative images were recorded using a phase-contrast microscope. Immunocytochemistry was used to verify the identities of CAFs and NFs. The CAFs and NFs cells suspended in BEGM were plated on glass coverslips. The cells were then incubated at 37°C for 24 h and immersed in 4% paraformaldehyde (PFA) for 15 min, washed with PBS and incubated in 10% normal goat serum (Boster) for 40 min to block nonspecific interactions, in the presence or absence of 0.3% Triton X-100 to permeabilise the cells. The coverslips were immersed in solutions containing primary antibodies (rabbit antihuman) for pan-cytokeratin (CK; 1:400; Abcam), vimentin (1:200; Abcam),  $\alpha$ -smooth muscle actin ( $\alpha$ -SMA; 1:200; Abcam) and fibroblast activation protein (FAP; 1:250; Abcam) and incubated at 4°C overnight. The cells were then treated with secondary antibodies (Jackson ImmunoResearch), either fluorescein isothiocyanate (FITC)-conjugated goat anti-rabbit IgG (H + L; 1:100) or Cy<sup>3</sup>-conjugated goat anti-rabbit IgG (1:100) for 1 h at 37°C. The cell nuclei were stained with 4',6'-diamidino-2-phenylindole (DAPI; Boster).

## 2.4 | Collection of culture supernatant and isolation of exosomes

Purified CAFs and NFs were cultured in BEGM medium (containing 10% exosome-depleted FBS) for 72 h. When each cell monolayer was near confluence, the culture supernatant was collected and centrifuged (1500 g, 10 min), followed by centrifugation (10,000 g, 30 min) at 4°C. The resulting exosome supernatant was then filtered (0.22  $\mu$ m filter) to eliminate cellular debris, followed by centrifugal ultrafiltration (Amicon<sup>®</sup> Ultra-15 100 KDa; Merck KGaA) to prevent potential contamination. Exosomes were isolated from the ultrafiltered supernatant with Ribo<sup>™</sup> Exosome Isolation Reagent (RiboBio Co., Ltd.), as previously described.<sup>15</sup> Briefly, the collected conditioned medium was mixed with Ribo<sup>™</sup> Exosome Isolation Reagent (ratio 3:1), followed by an incubation at 4°C overnight. The medium was then centrifuged (1500 g, 30 min), and the resulting exosome pellets were suspended in phosphate-buffered saline (PBS; HyClone; GE Healthcare Life Sciences) and analysed immediately or stored at -80°C for subsequent research.

## 2.5 | Transmission electron microscopy (TEM) and nanoparticle tracking analysis (NTA)

TEM was used to identify the morphological characteristics of exosome pellets, as described previously.<sup>15</sup> About 20  $\mu$ l of exosome-PBS solution was added to carbon-coated copper grids for 1 min, and then the excess solution was removed by blotting with filter paper. The exosome pellets were then stained with 20  $\mu$ l uranyl acetate dihydrate (2%) for about 1 min. The sample was finally dried for 10 min under a lamp before observation

with an FEI Tecnai G2 Spirit transmission electron microscope (FEI Company) operated at 80 kV. The particle size distribution was determined by NTA using a NanoSight NS300 instrument (Malvern Instruments, Inc.), in accordance with the operating instructions.

## 2.6 | Western blotting

Cell pellets and exosomes were lysed in RIPA lysis buffer. The protein concentration was determined, and protein samples from exosomes and control cells were separated by SDS polyacrylamide gel electrophoresis, followed by transfer to PVDF membranes (Millipore). The membranes were initially blocked with 5% nonfat milk and probed overnight with rabbit primary anti-CD63 (1:1000, Abcam), anti-TSG101 (1:2000, Abcam) and anti-Calnexin (1:2000, Abcam), followed by detection using horseradish peroxidase-conjugated goat anti-mouse/rabbit/rat IgG (1:2000; Jackson). Immunoreactive bands were detected using BeyoECL Plus (Beyotime Biotech). Beta-actin antibody (1:5,000; HuaAn Biotech) was used to normalise the amount of sample loaded.

## 2.7 | Extraction of total RNA

TRIzol reagent (Invitrogen; Thermo Fisher Scientific, Inc.) was used to extract high-quality total RNA from the exosomes obtained from each specimen. A NanoDrop 2000 spectrophotometer (NanoDrop Technologies; Thermo Fisher Scientific, Inc.) was used to analyse the concentration and quality of RNA. An Agilent 2200 Bioanalyser (Agilent Technologies, Inc.) was used to assess the RNA content.

## 2.8 | Small RNA (sRNA) sequencing and differential expression analysis

The sRNA next-generation sequencing technology was used to investigate differences in the miRNA profiles between exosomes from the three pairs of CAFs and NFs. The sRNA library preparation and sample sequencing were performed with the assistance of RiboBio Co., Ltd. using an Illumina HiSeq<sup>™</sup> 2500 device, as described previously.<sup>15</sup> Briefly, total RNA from the three pairs of CAF and NF exosomes was concatenated with 5'- and 3'-adaptors, followed by cDNA synthesis and PCR amplification. The cDNA library (18–40 nt) was then obtained by acrylamide gel purification, and single-end (SE) sequencing was conducted (1  $\times$  50 bp). The differential expression analysis of paired tests was performed using edgeR software with appropriate correction ( $|\log_2(\text{foldchange})| > 1, p < 0.05$ ) for multiple testing. The results are also shown in scatter, volcano and heat maps.

## 2.9 | RT-qPCR validation of selected miRNAs

We validated the sequencing results of the top 10 miRNAs (miR-16-5p, miR-29a-3p, miR-34c-5p, miR-32-5p, miR-490-5p, miR-193b-3p, miR-10a-3p, miR-656-3p, miR-19b-3p and miR-424-5p) in CAF-derived exosomes from all the three SLSCC patients by RT-qPCR. Total RNA was reversed-transcribed using RevertAid First Strand cDNA Synthesis Kit (Thermo Scientific, #K1622). The expression level of miRNA was measured using FastStart Universal SYBR Green Master(Rox) (Roche, #4913914001). All the procedures were performed following the manufacturer's instructions. The optimal PCR amplification procedures were as follows: pre-denaturation at 95°C for 30 s, cycling stage: 95°C for 15 s, 55–65°C for 10 s and 72°C for 30 s, 40 cycles; melt curve stage: 65–105°C. U6 snRNA was used as an internal control. The  $2^{-\Delta\Delta C_T}$  method was used to quantify the relative expression levels of selected miRNAs. The primers used are listed in Table 1.

## 2.10 | Identification of candidate exosomal miRNAs and target genes

The miRNAs that showed significant differences ( $p < 0.05$ ) between CAFs and NFs were selected as candidate exosomal miRNAs for

further analysis. The genes targeted by selective exosomal miRNAs were predicted by four online bioinformatic algorithms: TargetScan ([http://www.targetscan.org/vert\\_72/](http://www.targetscan.org/vert_72/)), miRDB (<http://mirdb.org>), miRTarBase (<http://mirtarbase.mbc.nctu.edu.tw/php/index.php>) and miRWalk (<http://mirwalk.umm.uni-heidelberg.de>). We selected an intersection among the four databases as a filtering condition to improve the accuracy of gene prediction. Only genes predicted simultaneously by specific exosomal miRNAs within the four databases were selected as target genes of the candidate exosomal miRNAs.

## 2.11 | Gene Ontology (GO) and Kyoto Encyclopaedia of Genes and Genomes (KEGG) analysis

The GO analysis (<http://www.geneontology.org/>) was used to predict the potential functions of the target genes of selected miRNAs, while the KEGG (<http://www.genome.jp/>) pathway enrichment analysis was performed to identify the predominant pathways based on the DAVID 6.7 online software (<http://david.abcc.ncifcrf.gov/home.jsp>). All GO terms and KEGG pathway enrichment analysis were analysed using kobas3.0 software (hypergeometric test/Fisher's exact test) with a  $p < 0.05$  threshold of significance, and the FDR correction method was Benjamini and Hochberg (Appendix S4).

TABLE 1 Sequences of primers used for quantitative real-time PCR

miRNA name	Primer sequence (5'→3')
miR-16-5p-R	CTCAACTGGTGTCTGGAGTCGGCAATTCAGTTGAGCGCCAATA
miR-16-5p-S	ACACTCCAGCTGGGTAGCAGCAGTAAATA
miR-29a-3p-R	CTCAACTGGTGTCTGGAGTCGGCAATTCAGTTGAGTAACCGAT
miR-29a-3p-S	ACACTCCAGCTGGGTAGCACCCTCTGAAAT
miR-34c-5p-R	CTCAACTGGTGTCTGGAGTCGGCAATTCAGTTGAGGCAATCAG
miR-34c-5p-S	ACACTCCAGCTGGGAGGCGAGTGTAGTTAGCT
miR-32-5p-R	CTCAACTGGTGTCTGGAGTCGGCAATTCAGTTGAGTGCAACTT
miR-32-5p-S	ACACTCCAGCTGGGTATTGCACATTACTAA
miR-490-5p-R	CTCAACTGGTGTCTGGAGTCGGCAATTCAGTTGAGACCCACCT
miR-490-5p-S	ACACTCCAGCTGGGCCATGGATCTCCAG
miR-193b-3p-R	CTCAACTGGTGTCTGGAGTCGGCAATTCAGTTGAGAGCGGGAC
miR-193b-3p-S	ACACTCCAGCTGGGAATGGCCCTCAAAGT
miR-10a-3p-R	CTCAACTGGTGTCTGGAGTCGGCAATTCAGTTGAGTATTTCCC
miR-10a-3p-S	ACACTCCAGCTGGGCAAATTCGTATCTAGG
miR-656-3p-R	CTCAACTGGTGTCTGGAGTCGGCAATTCAGTTGAGAGAGGTTG
miR-656-3p-S	ACACTCCAGCTGGGAATATTATACAGTCA
miR-19b-3p-R	CTCAACTGGTGTCTGGAGTCGGCAATTCAGTTGAGTCAGTTTT
miR-19b-3p-S	ACACTCCAGCTGGGTGTGCAAATCCATGCAA
miR-424-5p-R	CTCAACTGGTGTCTGGAGTCGGCAATTCAGTTGAGTTCAAAC
miR-424-5p-S	ACACTCCAGCTGGGCAGCAGCAATTCATGT
URP	TGGTGTCTGGAGTCTG
U6-S	CTCGCTTCGGCAGCACA
U6-A	AACGCTTACGAATTTGCGT

## 2.12 | Statistical analysis

Data were presented as the mean  $\pm$  standard deviation (SD) of at least three independent assays and analysed by Student's *t* test or Fisher's exact test.

All analyses were performed with the GraphPad Prism software version 6.00 for Windows (GraphPad Software). Values of  $p < 0.05$  were considered to indicate statistical significance.

## 3 | RESULTS

### 3.1 | Laryngoscopy, contrast-enhanced CT and pathology

Laryngoscopy revealed that all the three SLSCC tumours originated from the epiglottis and showed obvious enhancement in CT scans. Pathological examination showed that all tumours were moderately differentiated squamous cell carcinomas (Figure 1A–I).

### 3.2 | Primary culture, purification and morphology of CAFs and NFs

Although 10 pairs of CAFs and NFs from 10 SLSCC patients were initially subjected to primary culture, only three pairs were successfully cultured and purified due to contamination or poor propagation of the NFs *in vitro*. Two days after seeding, the CAFs, cancer cells and NFs grew out from the fragments. The CAFs and NFs were purified by differential trypsinization at passages 3–4. Purified CAFs and NFs were stored in liquid nitrogen. The morphology of the NFs showed small differences when compared with the CAFs. For example, fewer cell prominences were formed by the NFs than by the CAFs (Figure 2A–H). During subculture, the proliferation capacity of CAFs and NFs did not decrease significantly within seven consecutive passages. Therefore, CAFs and NFs between passages 3 and 6 were used for subsequent assays.

### 3.3 | Purity and identification of CAFs and NFs by immunofluorescence

Negative staining for pan-CK and positive staining for vimentin were detected in CAFs and NFs, confirming their fibroblast origin. The purity of CAFs and NFs revealed by vimentin staining was 100%, as validated by examining 10 randomly selected microscopic fields ( $\times 200$ ). In comparison with the NFs, CAFs also showed positive staining for FAP and  $\alpha$ -SMA, two CAF biomarkers (Figure 2I–R).

### 3.4 | Isolation and identification of exosomes derived from CAFs and NFs

Exosomes were verified by TEM, western blotting and NTA. TEM images showed the typical size range and morphology of

membrane-bound exosome particles, which were homogeneous in appearance (Figure 2S). Western blotting revealed positive expression of CD63 and TSG101, two of the well-established surface markers for exosomes, and negative expression of calnexin, commonly used as a negative control for extracellular vesicles<sup>16,17</sup> (Figure 2T). In addition, NTA analysis showed a size distribution (mean diameter at  $109.1 \pm 44.1$  nm) for the exosome particles that was consistent with the reported size range of exosomes (30–150 nm)<sup>18</sup> (Figure 2U).

### 3.5 | Different small RNA signatures of the exosome compartments derived from CAFs and NFs

Most of the exosomal clean reads could be mapped to known RNAs of the human genome, as illustrated in the circos plots (Figure S1). Analysis of the chromosomal location of all the mapped small RNAs indicated that they mainly originated from chromosomes 3, 5, 6, 7, 13 and 14. No significant differences were noted between CAFs and NFs for the distribution of the exosomal small RNA location in the genome (Figure S1A). Approximately, 12.3% of the miRNAs were common between CAFs-derived and NFs-derived exosomes (Figure S1B). The small RNA reads were functionally categorised based on a  $>90\%$  identity to exonic regions of the genome and annotated ncRNAs. Briefly, the miRNAs were the most abundant among the known sequences, followed by tRNAs, rRNA, snRNAs, snoRNA, Y RNAs, piRNAs and other RNAs that could not be categorised. Of all the small RNAs sequenced, an average of 67.61% of the miRNAs were detected in CAF-derived exosomes, compared with an average of 62.50% of the miRNAs in NF-derived exosomes (Figure S1C). Small RNAs, sized between 17 nt and 45 nt, were analysed. Most of the sequenced small RNAs were approximately 20 nt and 31 nt in size (clean reads) (Figure S1D). These characteristic sizes were consistent with small RNA populations.

### 3.6 | Aberrant expression profiles of exosomal miRNAs between CAFs and NFs

Patient YYX had 668 dysregulated miRNAs; however, only 45 miRNAs showed significant differences in expression. Of those, 3 were upregulated and 42 were downregulated ( $p < 0.05$ , Table S1). Patient XHG had 576 dysregulated miRNAs, but only 45 miRNAs showed significant differences in expression. Of those, 9 were upregulated and 36 were downregulated ( $p < 0.05$ , Table S2). Patient YSX had 476 dysregulated miRNAs, but only 33 miRNAs showed significant differences in expression. Of those, 8 were upregulated and 25 were downregulated ( $p < 0.05$ , Table S3). The results are also shown in scatter, volcano and heat maps (Figures 3A–F and 4A–C). Eleven miRNAs were downregulated simultaneously in two patients. Two miRNAs were upregulated simultaneously in two patients. Four miRNAs were downregulated simultaneously in all the three patients (Figure 6A, pie chart).

### 3.7 | RT-qPCR validation of top 10 miRNAs

In patient YYX, five of the top 10 CAF-derived exosomal miRNAs (miR-16-5p, miR-29a-3p, miR-34c-5p, miR-490-5p and miR-656-3p) were detected significantly downregulated by small RNA sequencing. Similarly, in patient XHG, seven of the top 10 CAF-derived exosomal miRNAs (miR-16-5p, miR-29a-3p, miR-32-5p, miR-10a-3p, miR-656-3p, miR-19b-3p and miR-424-5p) were significantly downregulated, and in patient YSX, six of

the top 10 miRNAs (miR-29a-3p, miR-34c-5p, miR-32-5p, miR-193b-3p, miR-656-3p and miR-424-5p) were significantly downregulated (Figure 4A-C, Tables S1-S3). As anticipated, the results of RT-qPCR detection revealed that the expression levels of these selected CAF-derived exosomal miRNAs were downregulated significantly ( $p < 0.05$ ,  $|\log_2(\text{foldchange})| > 1$ ) compared with the NF-derived exosomal miRNAs (Figure 5A-C). These findings indicated that the results of the small RNA sequencing were credible.

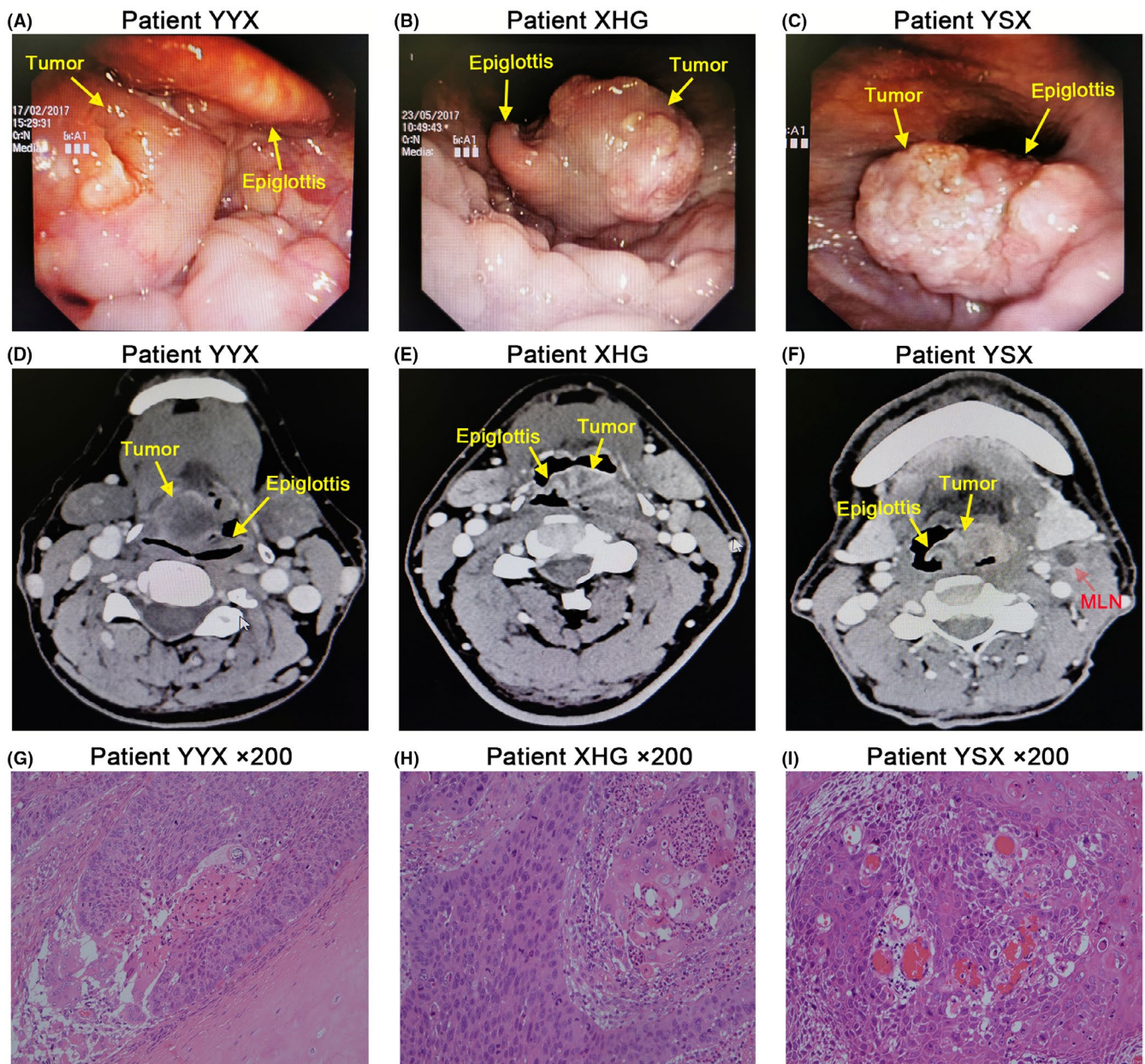


**FIGURE 1** Laryngoscopy, contrast-enhanced CT and pathology of tumours from patients with SLSCC. Typical laryngoscopic photos of tumours from patients (A) YYX, (B) XHG and (C) YSX. All the tumours in three patients originated from the epiglottis. Typical CT images of tumours from patients (D) YYX, (E) XHG and (F) YSX. An obvious metastatic lymph node (MLN) with liquefactive necrosis was observed in the left neck near the submandibular gland in patient YSX. Typical pathological images of tumours from patients (G) YYX, (H) XHG and (I) YSX. All three tumours were moderately differentiated squamous cell carcinomas

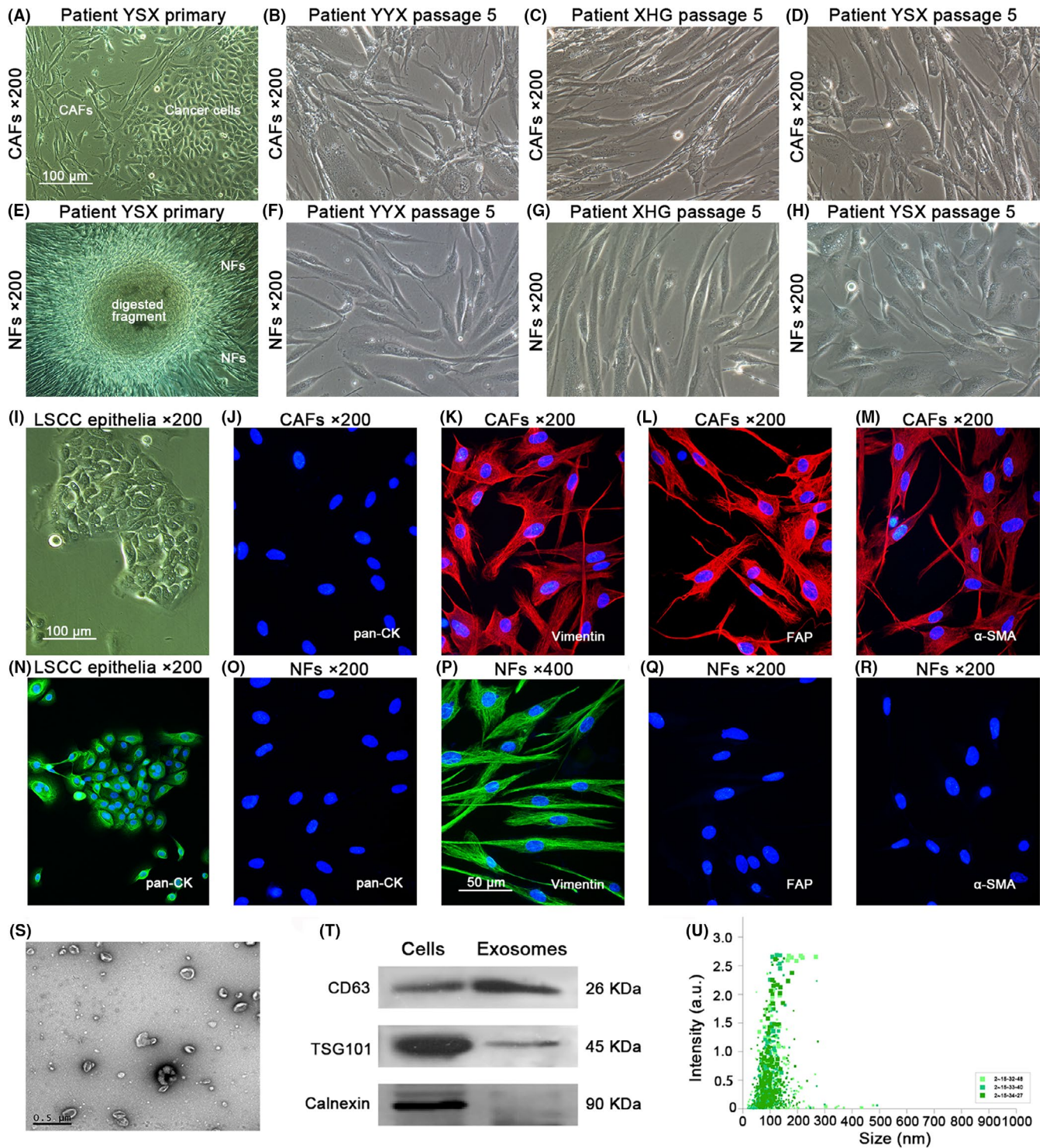


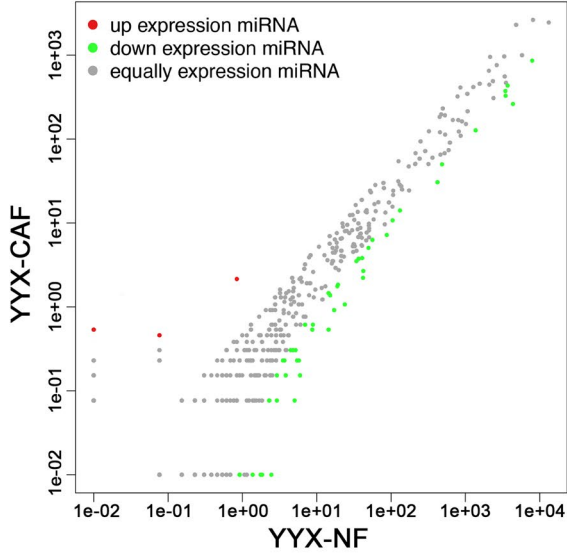
**FIGURE 2** Morphology and immunofluorescence of CAFs and NFs and identification of exosomes. (A) Primary CAFs co-existed with cancer cells. (B–D) Purified CAFs at passage 5 from 3 patients. (E) Primary NFs grew out from the collagenase-digested fragments. (F–H) Purified paired NFs at passage 5; the NFs showed fewer cell prominences compared with the CAFs. (I) Morphology of LSCC epithelia. (J–M) CAFs showed negative staining for pan-CK and positive staining for vimentin, FAP and  $\alpha$ -SMA. (N) Positive control of pan-CK. (O–R) NFs showed negative staining for pan-CK, FAP and  $\alpha$ -SMA and positive staining for vimentin. (S–U) TEM images, western blots and NTA data for exosomes

### 3.8 | Prediction of miRNAs target genes and GO and KEGG pathway enrichment analysis

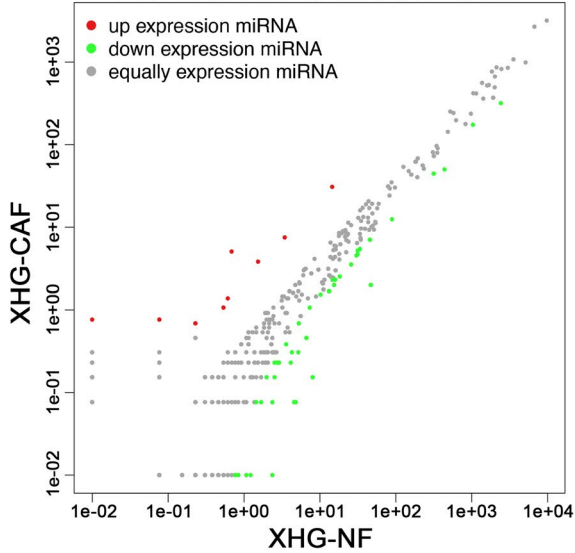
The GO approach used to explore potential gene functions revealed that all the GO terms were involved in three categories: biological

process, cellular component and molecular function. The top three biological processes (the lowest  $p$ -value,  $p < 0.05$ ) were related to regulation of transcription from the RNA polymerase II promoter, transcription from the RNA polymerase II promoter and positive regulation of RNA metabolic processes. The top three cellular

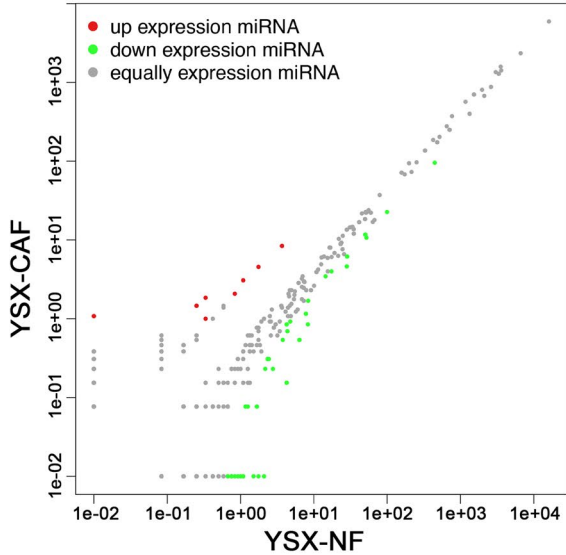
(A) The Difference of miRNA Profiles



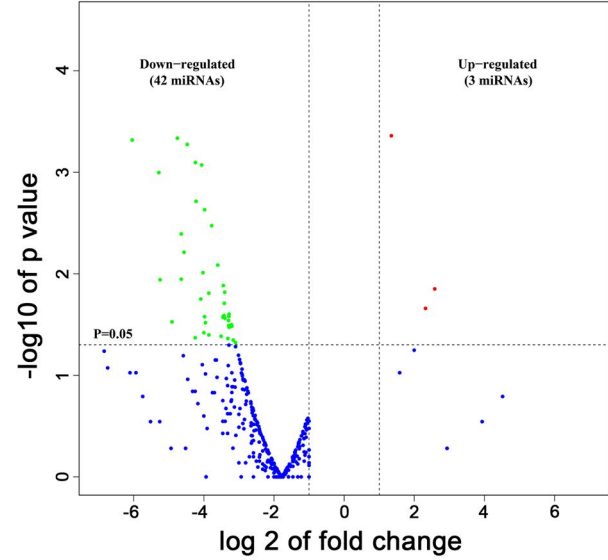
(B) The Difference of miRNA Profiles



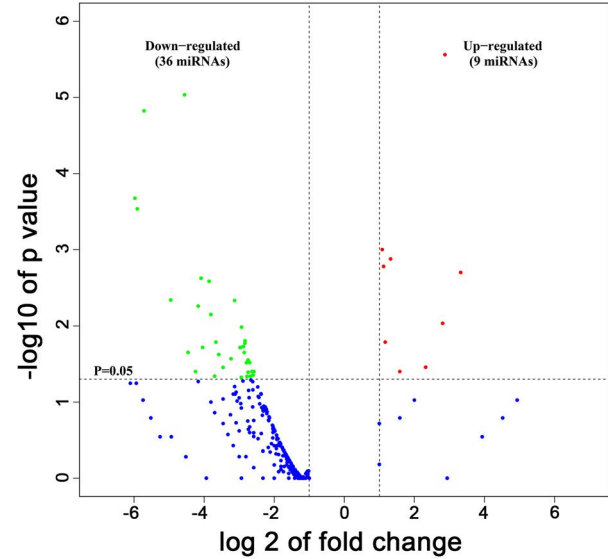
(C) The Difference of miRNA Profiles



(D) Patient YYX



(E) Patient XHG



(F) Patient YSX

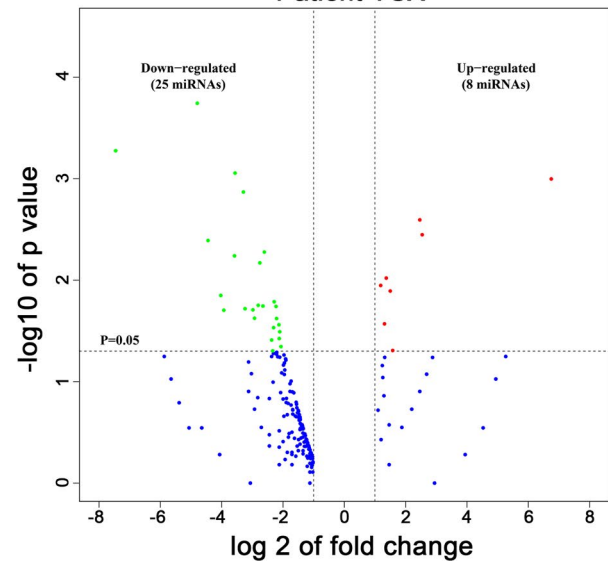


**FIGURE 3** Aberrant expression profiles of exosomal miRNAs between CAFs and NFs illustrated by scatter and volcano maps. (A–C) The scatter plot revealed the differential expression of exosomal miRNAs between CAFs and NFs. The inclusion criterion was  $|\log_2(\text{foldchange})| > 1$  and  $p < 0.05$ . (D–F) The volcano plot revealed the same expression profiles of exosomal miRNAs between CAFs and NFs. ( $|\log_2(\text{foldchange})| > 1, p < 0.05$ ). Red, upregulated; green, downregulated

components (the lowest  $p$ -value,  $p < 0.05$ ) were related to the RISC-loading complex, the micro-ribonucleoprotein complex and the RNAi effector complex. The top three molecular functions (the lowest  $p$ -value,  $p < 0.05$ ) were related to core promoter binding, regulatory region nucleic acid binding transcription factor activity and transcription regulatory region DNA binding (Figures 6B–D and 7A). The KEGG pathway enrichment analysis was performed to characterise the predominant pathways. The specific miRNA targets were compared to the whole reference gene background, and  $p < 0.05$  was chosen as the cut-off criterion. Thirty signalling pathways with the most statistical differences were selected and analysed (Figure 7B).

### 3.9 | Interaction networks of exosomal miRNAs and target genes

One miRNA can regulate hundreds of target genes, and one gene can be regulated by multiple miRNAs. An interaction network of selected exosomal miRNAs and genes was constructed. In all, 12 aberrantly expressed exosomal miRNAs were identified that formed a wide range of connections with the corresponding target genes. The top five were *miR-16-5p*, *miR-29a-3p*, *miR-34c-5p*, *miR-32-5p* and *miR-490-5p* (Figure 8A). The top five most common overlay genes were identified as *CCND1* (gene count 10), *CDKN1B* (gene count 7), *CDK6* (gene count 6), *PTEN* (gene count 5) and *FOS* (gene count 5) (Figure 8B, Table 2).

## 4 | DISCUSSION

Exosomal miRNAs may be derived from cancer cells themselves or from stromal cells like CAFs. To date, most studies have focused on exosomal miRNAs derived from cancer cells.<sup>19</sup> CAF-derived exosomal miRNAs are now receiving increasing attention, but no studies have yet been conducted to explore the aberrant expression profiles of exosomal miRNAs derived from CAFs in patients with SLSCC.

The present study is the first to describe dysregulation of the expression profile of miRNAs encapsulated in the CAF-derived exosomes in different patients with SLSCC. Three pairs of CAFs and NFs were successfully cultured and used for subsequent investigations. Laryngoscopy, CT scans and pathological examination showed that they were all moderately differentiated squamous cell carcinomas originated from the epiglottis (Figure 1A–I).

Both the CAFs and NFs showed long, fusiform morphology, with several cell prominences. However, the cell prominences were fewer on the NFs than on the CAFs, which probably reflected the fact that they were in a relatively inactive state (Figure 2A–H). After purification, the CAFs were distinguished from the NFs by positive

immunofluorescence staining for FAP and  $\alpha$ -SMA, two CAFs biomarkers (Figure 2I–R).

The collected exosomes were verified as such by TEM, western blotting and NTA (Figure 2S–U). Previous studies have reported that exosomes are generally enriched with certain specific marker proteins, such as CD9, CD63, CD81, TSG101 and HSP70,<sup>20</sup> with lower expression of some cellular proteins, such as cis-Golgi matrix protein GM130<sup>21</sup> and endoplasmic reticulum (ER) calnexin.<sup>16,17</sup> In the present study, the western blotting revealed the presence of CD63 and TSG101 and the absence of calnexin, consistent with the previously reported exosomes markers. The NTA analysis showed the exosome particles to have a size of  $109 \pm 44.1$  nm, consistent with the reported size range of exosomes (30–150 nm).<sup>22</sup> Our findings confirmed that these isolated particles qualified as exosomes.

The aberrant expression profiles of exosomal miRNAs derived from the three pairs of purified CAFs and NFs from patients with SLSCC were then analysed by next-generation sequencing (Table S1–S3, Figures 3A–F and 4A–C). Most of the aberrantly expressed miRNAs were downregulated, but a few were upregulated. Eleven miRNAs (*miR-452-5p*, *miR-651-5p*, *miR-16-5p*, *miR-424-5p*, *miR-378d*, *miR-32-5p*, *let-7i-3p*, *miR-16-2-3p*, *miR-136-3p*, *miR-221-5p* and *miR-34c-5p*) were downregulated simultaneously in two patients. Two miRNAs (*miR-184* and *miR-92a-1-5p*) were upregulated simultaneously in two patients. Interestingly, four exosomal miRNAs (*miR-656-3p*, *miR-655-3p*, *miR-337-5p* and *miR-29a-3p*) were downregulated simultaneously in all three patients (Figure 6A, pie chart).

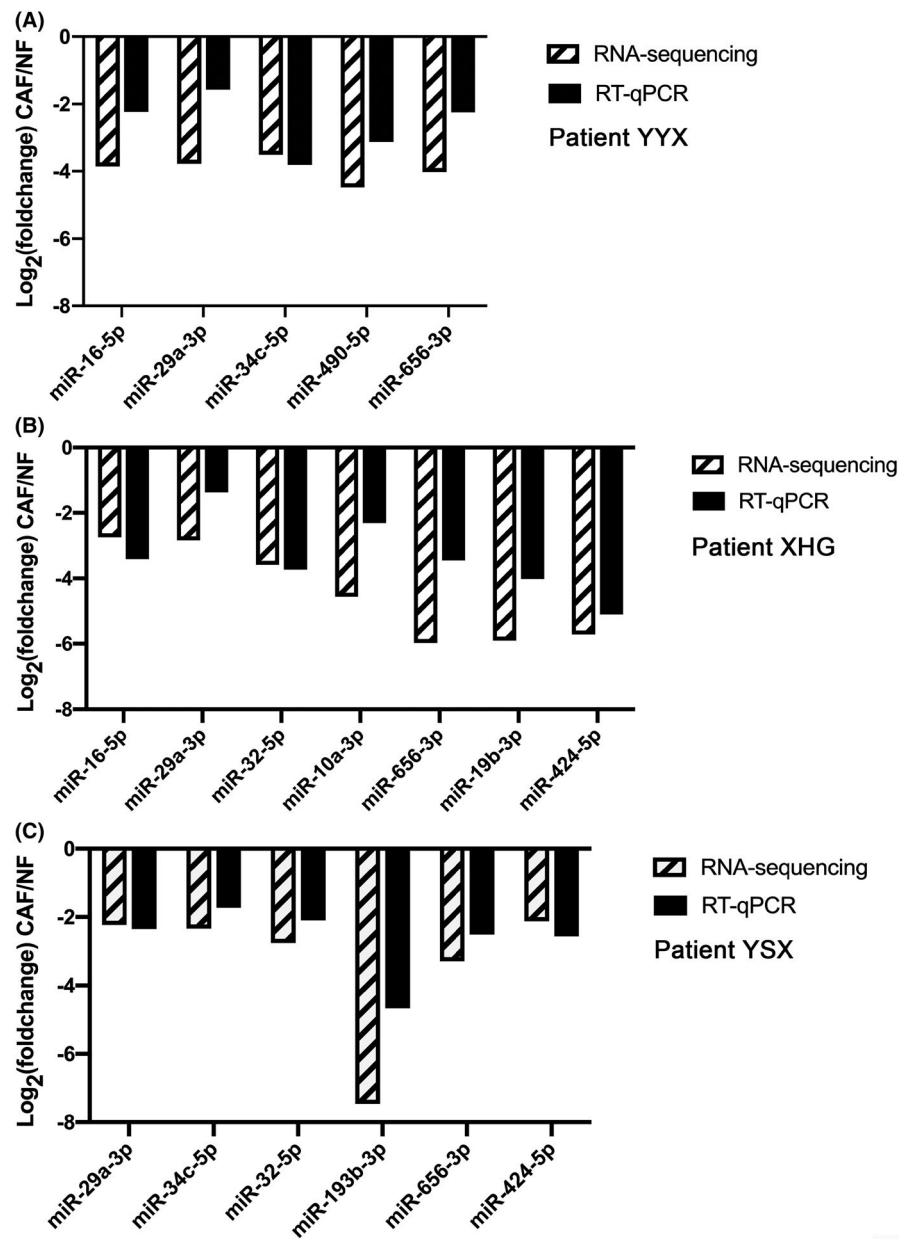
RT-qPCR was used to validate the results of sequencing of the top 10 miRNAs (*miR-16-5p*, *miR-29a-3p*, *miR-34c-5p*, *miR-32-5p*, *miR-490-5p*, *miR-193b-3p*, *miR-10a-3p*, *miR-656-3p*, *miR-19b-3p* and *miR-424-5p*). The results of RT-qPCR detection revealed that the expression levels of these selected CAF-derived exosomal miRNAs were downregulated significantly ( $p < 0.05$ ,  $|\log_2(\text{foldchange})| > 1$ ) compared with the NF-derived exosomal miRNAs (Figure 5A–C), which indicated that the results of the small RNA sequencing were credible.

The above-mentioned 11 miRNAs were downregulated simultaneously in two patients. However, the results of each miRNA in previous reports were controversial. For example, the expression of *miR-452-5p* was significantly increased in 387 clinical lung squamous cell carcinoma specimens,<sup>23</sup> whereas it was downregulated in 1007 prostate cancer samples.<sup>24</sup> A significant downregulation of *miR-32-5p* was reported in cervical cancer tissues and cells,<sup>25</sup> but a significant upregulation was detected in colorectal cancer tissues.<sup>26</sup> The two miRNAs that were upregulated simultaneously in two patients in our study have also had controversial findings. For example, *miR-184* expression was upregulated in renal carcinoma tissues,<sup>27</sup> but downregulated in endometrial carcinoma tissues.<sup>28</sup> These results suggest that these miRNAs play different regulatory



**FIGURE 4** Dysregulated expression profiles of exosomal miRNAs between CAFs and NFs (CAF/NF) illustrated by heat maps. The fold change of  $\log_2$  served as an inclusion criterion in either direction. Red signal: relative high expression; blue signal: relative low expression. (A) Patient YYX had 3 miRNAs that were upregulated and the other 42 were downregulated. (B) Patient XHG had 9 miRNAs that were upregulated and 36 that were downregulated. (C) Patient YSX had 8 miRNAs that were upregulated and 25 that were downregulated ( $p < 0.05$ )

**FIGURE 5** RT-qPCR validation of the top 10 miRNAs. RT-qPCR validation in (A) patient YYX, (B) patient XHG and (C) patient YSX. The results of RT-qPCR detection were very similar to those of next-generation sequencing ( $|\log_2(\text{foldchange})| > 1, p < 0.05$ ). U6 (RNU6-1) snRNA was used as an internal control



roles in different types of tumours. No studies have reported the regulation of miR-651-5p, miR-378d and miR-136-3p in cancer research, indicating that these three miRNAs may be promising targets for the intervention of LSCC.

The above-mentioned four exosomal miRNAs were downregulated simultaneously in all three patients, indicating that these miRNAs are closely related to the pathogenesis of LSCC. A few reports have appeared about miR-656-3p, miR-337-5p and miR-655-3p in different types of cancers.<sup>29-31</sup> However, all three miRNAs in these

reports were extracted either from tumour tissues or from cancer cell lines. None of the miRNAs were extracted from exosomes. MiR-29a-3p is a potential tumour-suppressive miRNA and is downregulated in papillary thyroid carcinoma tissues.<sup>32</sup> We found only one report that examined exosomal miR-29a-3p from oral squamous cell carcinoma cell lines.<sup>33</sup>

The bioinformatics analysis predicted the potential target genes of the exosome miRNAs that were differentially expressed between CAFs and NFs. Our exploration of the potential functions of these



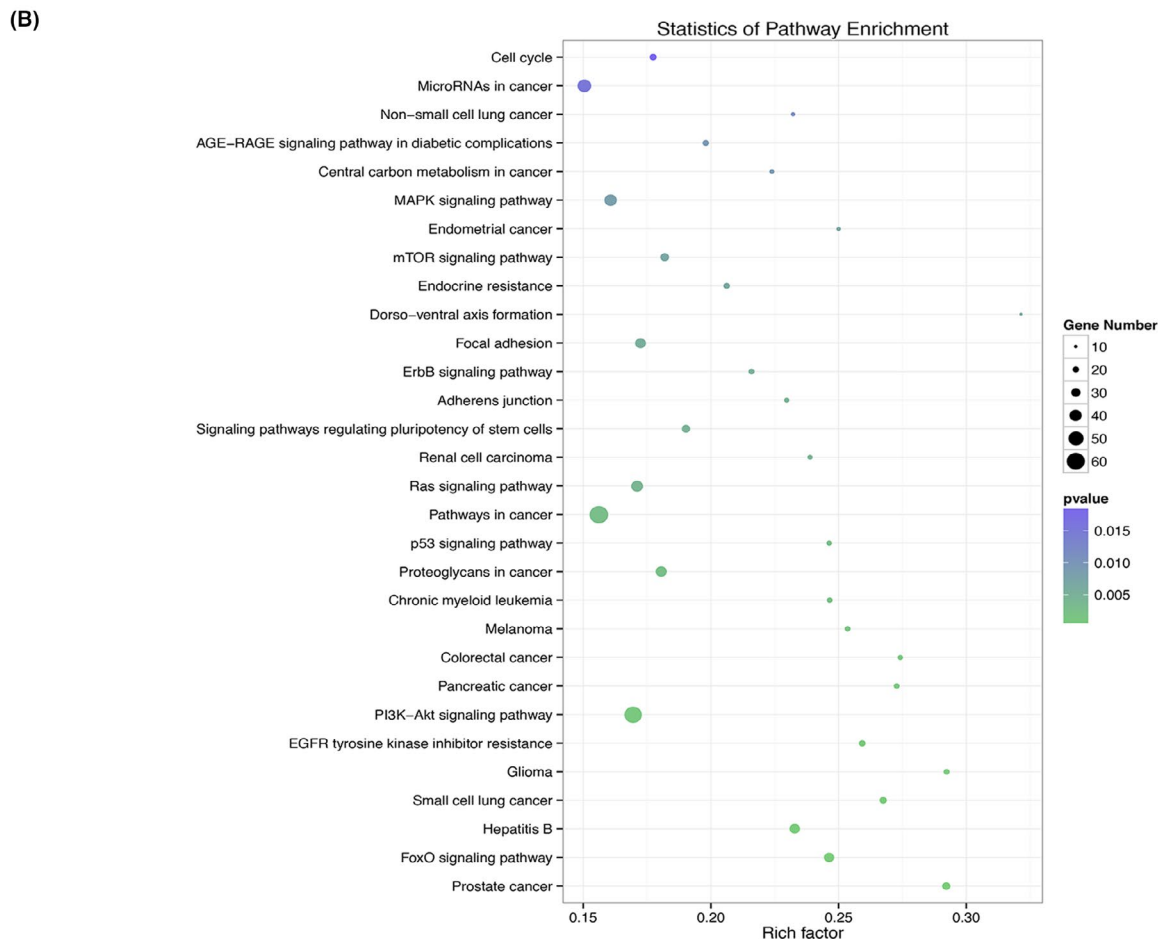
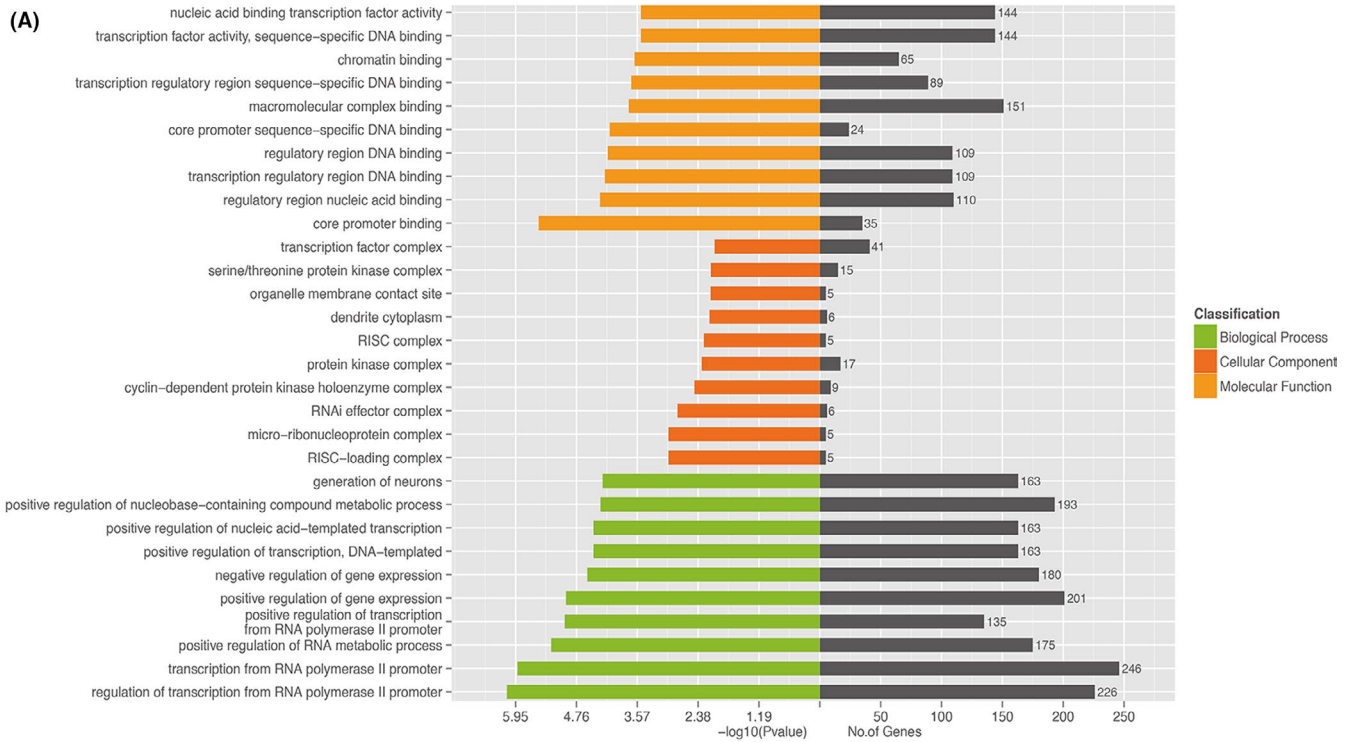


**FIGURE 7** The top 10 GO terms in three categories and KEGG pathway enrichment analysis. (A) The top 10 GO terms are illustrated for the three GO categories (biological process, cellular component and molecular function) ( $p < 0.05$ ). (B) Thirty signal pathways with greatest statistical differences were selected for the KEGG analysis ( $p < 0.05$ )

TABLE 2 Interaction of 10 selected genes with upstream miRNAs and downstream genes

miRNAs	miRNA count	Targeted genes	Genes interacted	Gene count	Sum
hsa-miR-10a-3p hsa-miR-29a-3p	2	IGF1	CCND1,FOS	2	4
hsa-miR-29a-3p hsa-miR-34c-5p	2	MYCN	CCND1,PTEN	2	4
hsa-miR-16-5p hsa-miR-424-5p	2	AGO4	CDK6,DICER1	2	4
hsa-miR-10a-3p hsa-miR-16-5p	2	CDC27	CCND1,CDKN1B,CBX2	3	5
hsa-miR-29a-3p hsa-miR-656-3p	2	CCND2	CCND1,CDKN1B,CDK6	3	5
hsa-miR-29a-3p hsa-miR-490-5p	2	FOS	CCND1,CDKN1B,IGF1,PTEN,NFE2L2	5	7
hsa-miR-19b-3p hsa-miR-29a-3p hsa-miR-32-5p	3	PTEN	CCND1,CDKN1B,MYCN,FOS,SYN1	5	8
hsa-miR-2682-5p hsa-miR-29a-3p hsa-miR-34c-5p	3	CDK6	CCND1,CDKN1B,CCND2,AGO4,CCNK,WEE1	6	9
hsa-miR-34c-5p hsa-miR-452-5p	2	CDKN1B	CCND1,CCND2,CDK6,FOS,YWHAZ,PTEN,CDC27	7	9
hsa-miR-193b-3p hsa-miR-424-5p	2	CCND1	CDKN1B,CCND2,CDK6,MYCN,BTG2,IGF1,FOS,PTE N,TLE1,CDC27	10	12

target genes using GO analysis revealed an involvement of three GO categories (Appendices S1–S3) that had transcription and regulation of RNA as important functions (Figures 6B–D and 7A). The KEGG pathway enrichment analysis identified the top 30 pathways involved in many types of cancers, in critical signalling pathways in cancer initiation and progression and in regulation of the cell cycle (Figure 7B). These abnormal GO categories and KEGG signalling pathways may be related to the pathogenesis and cancer biology of LSCC.

We also constructed an interaction network of selected exosomal miRNAs and target genes. This network contained 12 aberrantly expressed exosomal miRNAs that formed a wide range of connections with the corresponding target genes (Figure 8A). Of these, the top five miRNAs were miR-16-5p, miR-29a-3p, miR-34c-5p, miR-32-5p and miR-490-5p. All these five miRNAs were reportedly downregulated in breast cancer,<sup>34</sup> thyroid carcinoma,<sup>32</sup> osteosarcoma,<sup>35</sup> renal cell carcinoma tissues<sup>36</sup> and cervical cancer tissues and cells.<sup>25</sup> Our findings indicated that these top five miRNAs may play a critical role in the tumorigenesis of LSCC.

The top five most common overlay genes were identified as CCND1 (gene count 10), CDKN1B (gene count 7), CDK6 (gene count 6), PTEN (gene count 5) and FOS (gene count 5) through interaction network analysis (Figure 8B, Table 2). Of these, CCND1, CDKN1B and CDK6 are critical regulatory subunits required for the cell cycle

G1/S transition. Dysfunction of these three genes may, therefore, lead to uncontrolled cell cycle progression and ultimately to tumourigenesis.<sup>37,38</sup> These critical findings indicate that the pathogenesis of supraglottic laryngeal cancer may be cell cycle disorder.

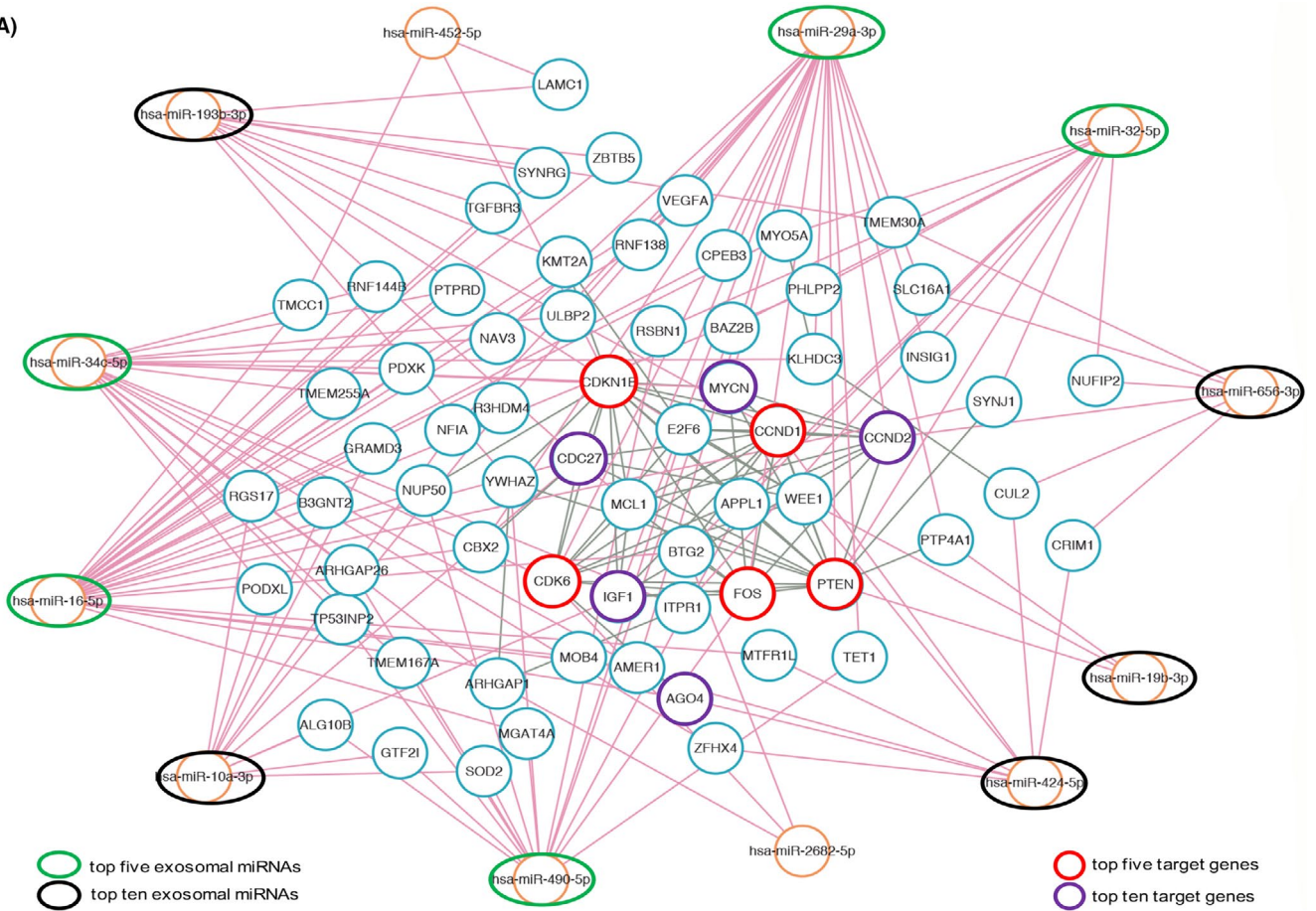
Most of the previously reported exosomal miRNAs were cancer cell-derived. Although increasing studies focused on the exosomal miRNAs extracted from CAFs, almost none of them were conducted using exosomal miRNAs derived from CAF primary cultures from different patients. We believe that the miRNAs with the most significant statistical difference or showing the same expression trends in more than one patient sample are the miRNAs that jointly constitute a carcinogenic TME and play decisive roles in the initiation and progression of SLSCC.

## 5 | CONCLUSION

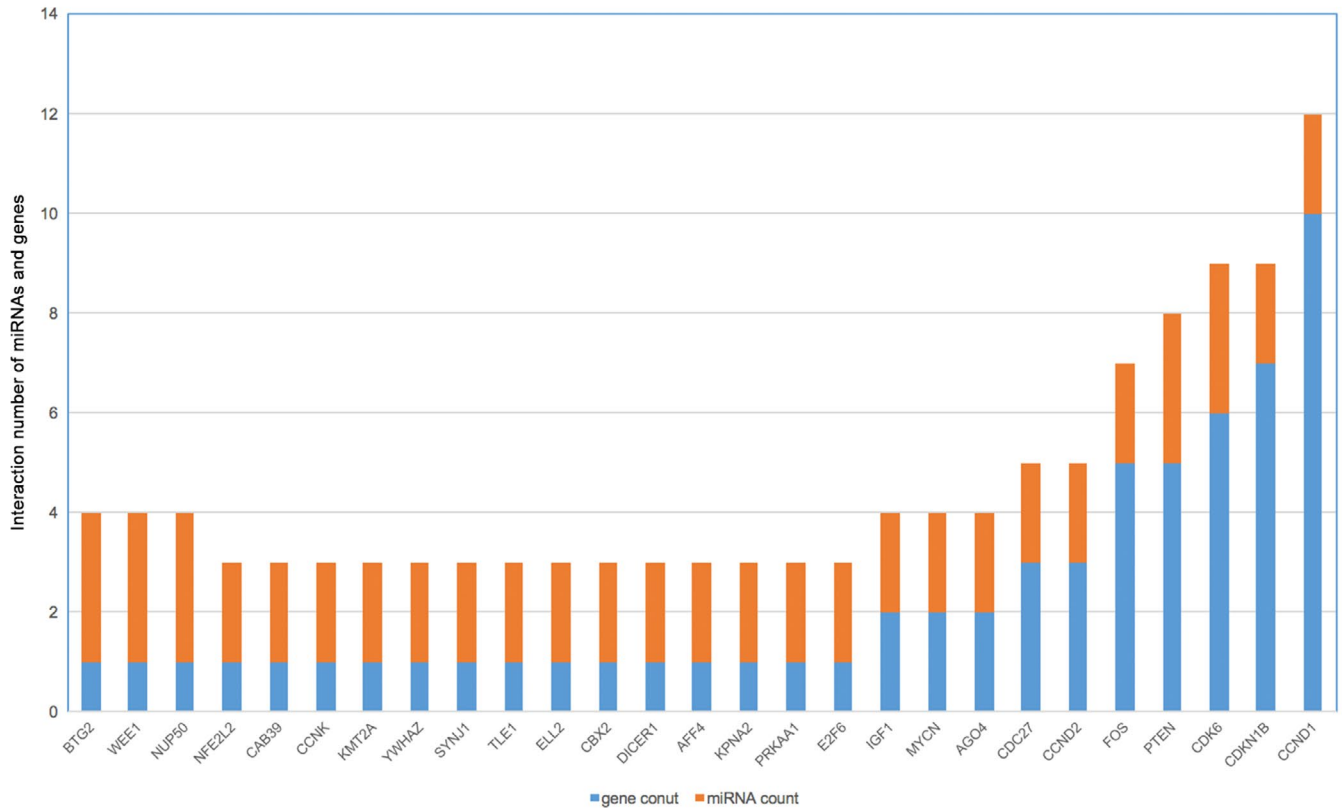
In this study, the aberrant expression profile of CAF-derived exosomal miRNAs from three moderately differentiated supraglottic LSCC patients was identified by next-generation sequencing. The top five miRNAs, miR-16-5p, miR-29a-3p, miR-34c-5p, miR-32-5p and miR-490-5p, and the top five most common overlay target genes, CCND1, CDKN1B, CDK6, PTEN and FOS, were revealed.

FIGURE 8 Interaction network of exosomal miRNAs and target genes. (A) The network revealed the interactions between 12 identified exosomal miRNAs and target genes determined by Cytoscape. (B) The interaction number of the selected genes with upstream miRNAs and downstream target genes. The orange bars represent the number of upstream miRNAs that regulate the present gene (such as CCND1, 2 upstream miRNAs). The blue bars indicate the number of downstream target genes that interacted with the present gene (such as CCND1, 10 downstream target genes)

(A)



(B)



These critical miRNAs and target genes are mainly related to cell cycle regulation, indicating that the pathogenesis of supraglottic carcinoma may be cell cycle disorder. Therefore, they may represent promising biomarkers for therapeutic intervention. However, these predictions require further experimental exploration in future studies.

## ACKNOWLEDGEMENTS

This study was supported by grants from the National Natural Science Foundations of China (grant no. 81972529) and grants from Natural Science Foundation of Shanghai University of Traditional Chinese Medicine (grant no. 2019LK029). The funders had no role in study design, data collection and analysis, decision to publish or preparation of the manuscript.

## CONFLICT OF INTEREST

The authors indicated no potential conflicts of interest.

## AUTHOR CONTRIBUTIONS

CPW, MW and LZ conceived and designed the study. CPW, QH and CYH performed the experiments. CPW, MW, YG and HLG analysed the data. CPW and MW wrote the manuscript. YG, HLG and LZ reviewed and edited the manuscript. All authors read and approved the final manuscript.

## ETHICAL APPROVAL

SLSCC specimens were obtained with the approval of the Ethics Committee of the Eye, Ear, Nose and Throat Hospital, Fudan University, Shanghai, China. Signed informed consents were obtained from all patients included in this study.

## DATA AVAILABILITY STATEMENT

All the data related to this work are available at the corresponding author.

## ORCID

Liang Zhou  <https://orcid.org/0000-0002-8588-2959>

## REFERENCES

- Patel TD, Echanique KA, Yip C, et al. Supraglottic squamous cell carcinoma: a population-based study of 22,675 cases. *Laryngoscope*. 2019;129(8):1822-1827.
- Casey SC, Amedei A, Aquilano K, et al. Cancer prevention and therapy through the modulation of the tumor microenvironment. *Semin Cancer Biol*. 2015;35(Suppl):S199-s223.
- Sidaway P. Breast cancer: fibroblast subtypes alter the microenvironment. *Nat Rev Clin Oncol*. 2018;15(5):264-265.
- Hu JL, Wang W, Lan XL, et al. CAFs secreted exosomes promote metastasis and chemotherapy resistance by enhancing cell stemness and epithelial-mesenchymal transition in colorectal cancer. *Mol Cancer*. 2019;18(1):91.
- Azmi AS, Bao B, Sarkar FH. Exosomes in cancer development, metastasis, and drug resistance: a comprehensive review. *Cancer Metastasis Rev*. 2013;32(3-4):623-642.
- Yang F, Ning Z, Ma L, et al. Exosomal miRNAs and miRNA dysregulation in cancer-associated fibroblasts. *Mol Cancer*. 2017;16(1):148.
- Shan G, Zhou X, Gu J, et al. Downregulated exosomal microRNA-148b-3p in cancer associated fibroblasts enhance chemosensitivity of bladder cancer cells by downregulating the Wnt/ $\beta$ -catenin pathway and upregulating PTEN. *Cell Oncol (Dordr)*. 2021;44(1):45-59.
- Liu Y, Yang Y, Du J, et al. MiR-3613-3p from carcinoma-associated fibroblasts exosomes promoted breast cancer cell proliferation and metastasis by regulating SOCS2 expression. *IUBMB Life*. 2020;72(8):1705-1714.
- Takeuchi T, Kawasaki H, Luce A, et al. Insight toward the microRNA profiling of laryngeal cancers: biological role and clinical impact. *Int J Mol Sci*. 2020;21(10):3693.
- Li P, Liu H, Wang Z, et al. MicroRNAs in laryngeal cancer: implications for diagnosis, prognosis and therapy. *Am J Transl Res*. 2016;8(5):1935-1944.
- Zhao Q, Zheng X, Guo H, et al. Serum exosomal miR-941 as a promising oncogenic biomarker for laryngeal squamous cell carcinoma. *J Cancer*. 2020;11(18):5329-5344.
- Wang J, Zhou Y, Lu J, et al. Combined detection of serum exosomal miR-21 and HOTAIR as diagnostic and prognostic biomarkers for laryngeal squamous cell carcinoma. *Med Oncol*. 2014;31(9):148.
- Du HD, Wu CP, Zhou L, et al. Separation and cultivation of laryngeal carcinoma-associated fibroblasts and biological influence on a laryngeal carcinoma cell line. *Acta Otolaryngol*. 2013;133(7):755-760.
- Wang M, Wu CP, Pan JY, et al. Cancer-associated fibroblasts in a human HEp-2 established laryngeal xenografted tumor are not derived from cancer cells through epithelial-mesenchymal transition, phenotypically activated but karyotypically normal. *PLoS One*. 2015;10(2):e0117405.
- Huang Q, Yang J, Zheng J, et al. Characterization of selective exosomal microRNA expression profile derived from laryngeal squamous cell carcinoma detected by next generation sequencing. *Oncol Rep*. 2018;40(5):2584-2594.
- Lässer C, O'Neil SE, Ekerljung L, et al. RNA-containing exosomes in human nasal secretions. *Am J Rhinol Allergy*. 2011;25(2):89-93.
- Li X, Li X, Lin J, et al. Exosomes derived from low-intensity pulsed ultrasound-treated dendritic cells suppress tumor necrosis factor-induced endothelial inflammation. *J Ultrasound Med*. 2019;38(8):2081-2091.
- Schageman J, Zeringer E, Li M, et al. The complete exosome workflow solution: from isolation to characterization of RNA cargo. *Biomed Res Int*. 2013;2013:253957.
- Wang M, Yu F, Ding H, et al. Emerging function and clinical values of exosomal microRNAs in cancer. *Mol Ther Nucleic Acids*. 2019;16:791-804.
- Zhang G, Chen L, Guo X, et al. Comparative analysis of microRNA expression profiles of exosomes derived from normal and hypoxic preconditioning human neural stem cells by next generation sequencing. *J Biomed Nanotechnol*. 2018;14(6):1075-1089.
- Lotvall J, Hill AF, Hochberg F, et al. Minimal experimental requirements for definition of extracellular vesicles and their functions: a position statement from the international society for extracellular vesicles. *J Extracell Vesicles*. 2014;3:26913.
- Zeringer E, Barta T, Li M, et al. Strategies for isolation of exosomes. *Cold Spring Harb Protoc*. 2015;2015(4):319-323.
- Gan XN, Gan TQ, He RQ, et al. Clinical significance of high expression of miR-452-5p in lung squamous cell carcinoma. *Oncol Lett*. 2018;15(5):6418-6430.
- Gao L, Zhang LJ, Li SH, et al. Role of miR-452-5p in the tumorigenesis of prostate cancer: a study based on the cancer genome atl(TCGA), gene expression omnibus (GEO), and bioinformatics analysis. *Pathol Res Pract*. 2018;214(5):732-749.
- Liu YJ, Zhou HG, Chen LH, et al. MiR-32-5p regulates the proliferation and metastasis of cervical cancer cells by targeting HOXB8. *Eur Rev Med Pharmacol Sci*. 2019;23(1):87-95.

26. Liang H, Tang Y, Zhang H, et al. MiR-32-5p regulates radiosensitization, migration and invasion of colorectal cancer cells by targeting TOB1 gene. *Onco Targets Ther.* 2019;12:9651-9661.
27. Yang J, Lai CC, Xian ZM, et al. Preliminary results indicate increased expression of miR-184 in patients with renal carcinoma. *Eur Rev Med Pharmacol Sci.* 2019;23(16):6878-6887.
28. Chen Z, Zhu Y, Fan X, et al. Decreased expression of miR-184 restrains the growth and invasion of endometrial carcinoma cells through CDC25A-dependent Notch signaling pathway. *Am J Transl Res.* 2019;11(2):755-764.
29. Chen T, Qin S, Gu Y, et al. Long non-coding RNA NORAD promotes the occurrence and development of non-small cell lung cancer by adsorbing MiR-656-3p. *Mol Genet Genomic Med.* 2019;7(8):e757.
30. Molina-Pinelo S, Carnero A, Rivera F, et al. MiR-107 and miR-99a-3p predict chemotherapy response in patients with advanced colorectal cancer. *BMC Cancer.* 2014;14:656.
31. Zha JF, Chen DX. MiR-655-3p inhibited proliferation and migration of ovarian cancer cells by targeting RAB1A. *Eur Rev Med Pharmacol Sci.* 2019;23(9):3627-3634.
32. Ma Y, Sun Y. miR-29a-3p inhibits growth, proliferation, and invasion of papillary thyroid carcinoma by suppressing NF- $\kappa$ B signaling via direct targeting of OTUB2. *Cancer Manag Res.* 2018;11:13-23.
33. Cai J, Qiao B, Gao N, et al. Oral squamous cell carcinoma-derived exosomes promote M2 subtype macrophage polarization mediated by exosome-enclosed miR-29a-3p. *Am J Physiol Cell Physiol.* 2019;316(5):C731-C740.
34. Ruan L, Qian X. MiR-16-5p inhibits breast cancer by reducing AKT3 to restrain NF- $\kappa$ B pathway. *Biosci Rep.* 2019;39(8):BSR20191611.
35. Wang Y, Wang X, Tang J, et al. The study of mechanism of miR-34c-5p targeting FLOT2 to regulate proliferation, migration and invasion of osteosarcoma cells. *Artif Cells Nanomed Biotechnol.* 2019;47(1):3559-3568.
36. Chen K, Zeng J, Tang K, et al. miR-490-5p suppresses tumour growth in renal cell carcinoma through targeting PIK3CA. *Biol Cell.* 2016;108(2):41-50.
37. VanArsdale T, Boshoff C, Arndt KT, et al. Molecular pathways: targeting the cyclin D-CDK4/6 axis for cancer treatment. *Clin Cancer Res.* 2015;2(13):2905-2910.
38. Cusan M, Mungo G, De Marco Zompit M, et al. Landscape of CDKN1B mutations in luminal breast cancer and other hormone-driven human tumors. *Front Endocrinol (Lausanne).* 2018;9:393.

#### SUPPORTING INFORMATION

Additional supporting information may be found in the online version of the article at the publisher's website.

**How to cite this article:** Wu C, Wang M, Huang Q, et al. Aberrant expression profiles and bioinformatic analysis of CAF-derived exosomal miRNAs from three moderately differentiated supraglottic LSCC patients. *J Clin Lab Anal.* 2022;36:e24108. <https://doi.org/10.1002/jcla.24108>